Explicit matrices for a composite beam-column with refined zigzag kinematics

PAPER • OPEN ACCESS

Conceptual design of a modular EC heating system for EU-DEMO

OPEN ACCESS
IOP Publishing | International Atomic Energy Agency
Nuclear Fusion
Nucl. Fusion **64** (2024) 106003 (15pp)
https://doi.org/10.1088/1741-4326/ad66e3

Conceptual design of a modular EC heating system for EU-DEMO

Alessandro Bruschi[1,*], Jean-Philippe Hogge[2], John Jelonnek[3], Dirk Strauss[4], Chuanren Wu[3], Gaetano Aiello[4], Kostas Avramidis[5], Benedetta Baiocchi[1], Daniel Birlan[2], René Chavan[2], Ioannis Chelis[5], Arnaud Clement[2], Aldo Collaku[6], Fabien Crisinel[2], Rosa Difonzo[6], Benjamin Ell[3], Francesco Fanale[7], Pierluigi Fanelli[8], Lorenzo Figini[1], Eleonora Gajetti[6], Gerd Gantenbein[3], Saul Garavaglia[1], Timothy P. Goodman[2], Stefan Illy[3], Zisis Ioannidis[9], Jambo Jin[3], George Latsas[5], Cinta L. Marraco Borderas[2], Stefan Marsen[10], Alessandro Moro[1], Marc Noël[2], Dimitrios Peponis[5], Tonio Pinna[7], Paola Platania[1], Natale Rispoli[1], Tobias Ruess[3], Tomasz Rzesnicki[3], Alessandra Salvitti[8], Laura Savoldi[6], Theo Scherer[4], Sabine Schreck[4], Alessandro Simonetto[1], Peter Spaeh[4], Sebastian Stanculovic[3], Torsten Stange[10], Manfred Thumm[3], Ioannis Tigelis[5], Christos Tsironis[11], Dietmar Wagner[12] and Anastasia Xydou[2]

[1] Institute for Plasma Science and Technology, National Research Council (ISTP-CNR), Milano, Italy
[2] Swiss Plasma Center (SPC), EPFL, Lausanne, Switzerland
[3] IHM, Karlsruhe Institute of Technology (KIT), Karlsruhe, Germany
[4] IAM-AWP, Karlsruhe Institute of Technology (KIT), Karlsruhe, Germany
[5] Department of Physics, National and Kapodistrian University of Athens, Zografou, Athens, Greece
[6] MAHTEP Group, Dipartimento Energia 'Galileo Ferraris', Politecnico di Torino, Torino, Italy
[7] ENEA, Fusion and Nuclear Safety Department, C.R. Frascati, Frascati, Italy
[8] Department of Economy, Engineering, Society and Business (DEIm), University of Tuscia, Viterbo, Italy
[9] Department of Aerospace Science and Technology, National and Kapodistrian University of Athens, Athens, Greece
[10] Max-Planck-Institute for Plasma Physics, Greifswald, Germany
[11] School of Electrical and Computer Engineering, National Technical University of Athens, Athens, Greece
[12] Max-Planck-Institute for Plasma Physics, Garching, Germany

E-mail: alessandro.bruschi@istp.cnr.it

Received 22 February 2024, revised 14 June 2024
Accepted for publication 24 July 2024
Published 14 August 2024

Abstract

The European DEMO (EU-DEMO) reactor studies within EUROfusion aim to develop a fusion power plant concept. The large tokamak device needs an auxiliary heating power which, at the present stage, is provided by the Electron Cyclotron (EC) heating system with up to 130 MW foreseen to reach different regions of plasma for heating, suppression of instabilities and the possibility to support ramp-up and ramp-down phases. The present conceptual design of the

* Author to whom any correspondence should be addressed.

system is based on 2 MW coaxial-cavity gyrotron sources, a transmission line (TL) using both circular corrugated waveguides and quasi-optical evacuated multi-beam TLs, and mirror antennas located in the Equatorial Port. In order to create a modular system, the sources are grouped in 'clusters', whose powers are combined in the quasi-optical TL, up to the tokamak building, where they are split and routed as single waveguides. In the launcher, they are combined together again on the launching mirrors, to save space for the apertures in the Breeding Blanket. The present EC heating system has a certain flexibility to adapt to changing design guidelines. The development status of the system is presented.

Keywords: EC heating system, DEMO, multi-beam transmission line

(Some figures may appear in colour only in the online journal)

1. Introduction

The design and construction of the European DEMO reactor is a major step of the EUROfusion roadmap [1], and has the aim of developing the concept for a commercial fusion power plant within the half of this century [2]. At the pre-conceptual design stage [3] DEMO is conceived as a large tokamak device with long plasma pulses (2 h) and with an auxiliary heating power of 130 MW [4]. Waiting for a decision on the heating mix, this power could be provided by Electron Cyclotron (EC) heating alone. This is the baseline for the conceptual design of the EC system started in 2021 [5].

1.1. EC heating system main tasks and requirements

The main tasks to be provided by the EC system are [4]:

- assisted plasma break-down
- bulk plasma heating during plasma current ramp-up to burn, and ramp down
- radiative instability (RI) control
- temperature control of core plasma during burn phase.
- Control of Magneto Hydro Dynamic (MHD) instabilities as sawteeth and Neoclassical Tearing Modes (NTM) by localized current drive (CD)
- Plasma CD (optional).

The EC power should be provided independently for three main tasks, as is summarized in table 1.

It consists of at least 30 MW for Bulk Heating (BH) deposited in the plasma center, 30 MW in narrow beams at the (variable) location of the 2:1 and 3:2 NTM instabilities, and additional 70 MW ready to be launched at the plasma edge for counteracting the RI in case of tungsten impurity influx [3]. The additional but necessary tasks, such as Plasma Breakdown, Ramp-up and Ramp-down assistance are provided by a part or all of the power available. Currently, CD by the EC system is not required: nevertheless, the conceptual design is flexible to provide a certain amount of plasma CD, if required in the future.

Table 1. Main tasks assigned to the EC heating system.

Task	Location	Power
Bulk heating	Plasma center	30 MW
NTM control	Mid-radius ($q = 1.5$ and 2)	30 MW
RI control	Plasma edge	70 MW

1.2. EC heating system concept

On the basis of these requirements, the present concept of the EC system has been developed in previous years [6], and the design updated for the DEMO 2018 version [7]. The power generation system is based on 2 MW coaxial-cavity gyrotron sources, grouped in 'clusters'. The Transmission Line (TL) concept foresee a mixed quasi-optical and waveguide line. The output power of each gyrotron is transmitted by evacuated waveguides (EWGs) to a set of mirrors which combine the power of a cluster in a set of parallel beams, running together toward the tokamak building in an underground corridor, in a quasi-optical evacuated TL. Another set of mirrors near the tokamak building separates and launches the beams into circular corrugated waveguides running close to the ceiling in the DEMO gallery at the equatorial level, up to the Equatorial Port, in which fixed and movable mirror antennas launch these beams into the plasma. In the next sections the different parts of the system will be described.

2. System design guidelines

Since the reference tokamak (and plasma) parameters, and the requirements of power and availability are not final but subject to updates in the next future, the EC system has been conceived to be as modular as possible, with a flexibility in terms of power directed to the different plasma regions, frequency, number of lines and ports.

2.1. Operating frequencies and design variants

The current EC heating system design with the variants here described is made according to the DEMO 2018 baseline [7], with major radius of 9.07 m, aspect ratio of 3.1 and central

magnetic field of 5.87 T. Foreseen changes toward a lower aspect ratio plasma are not considered in this paper. For the different plasma locations to be reached by the EC waves to fulfill the requirements of section 1.1, the number of frequencies for injection has to be at least two, possibly three. For keeping enough flexibility in the system, the multi-purpose/multi-frequency gyrotrons under development are capable to be operated at different frequencies. Those operating frequencies are selected as consecutive multiples of the $\lambda_D/2$ resonance frequency of the Chemical Vapor Deposited (CVD) diamond disk output window where λ_D is the wavelength in the dielectric (diamond). If considering the same window thickness as for the ITER gyrotrons and a center frequency of 170 GHz, the possible operating frequencies are 136, 170, 204 and 238 GHz, with the first three as the frequencies under consideration for the EC heating system design.

2.2. Fixed frequency variant

The reference operating mode of the EC launcher is defined as the 'fixed-frequency' (FF) variant. Since the stabilization of NTMs requires injection of power located at the $q = 1.5$ and $q = 2$ plasma rational surfaces, whose location may vary in time following changes in the plasma current profile, at a fixed injection frequency the stabilization task requires an EC launcher with beam steering capabilities. This can be realized by means either of a Remote-Steerable (RS) waveguide antenna [8] or of movable mirrors in the launcher, guided to follow the NTM variable location in the plasma.

A RS antenna for EU-DEMO has been studied in former times [9], but it was found not ideal due to the large required openings [10] that would cause a higher than sustainable neutron loading on the toroidal field coils [11]. Also, the poor focalization properties of the mm-wave beam from the RS antenna alone would result in power/current deposition widths in the plasma too large for the needs [12].

The need of narrow beams for NTM stabilization led to studies on the possibility to use multiple open-ended waveguides and front-steering mirrors, and finally to the chosen design, consisting of a 'Mid-Steering' Antenna (MSA) in which a movable mirror recessed behind the Breeding Blanket (BB) is foreseen for NTM suppression beams [7]. The drawback of this solution is the presence of movable parts in the port, that are subject to high neutron fluxes, being placed close to the plasma edge, even partially protected by the BB [13]. These movable parts may be subject to higher stresses and more frequent need for replacement, increasing the operational cost.

2.3. Tuneable frequency (TF) variant

To overcome this drawback, a TF variant is under consideration to select finely the plasma deposition location without using movable mirrors. The target is to be able to tune in a few seconds the operating frequency of a gyrotron in steps of 2–3 GHz for a range of about ± 10 GHz around a main frequency, in order to span the deposition location around the range of position corresponding to the main NTM modes.

A specific study [14] based on a simple sweeping strategy of the EC frequency and on reasonable assumptions on gyrotrons and launching parameters demonstrate that NTM stabilization using frequency step-tuneable EC injection is achievable in principle. To reach the goal, further investigation is required, given the uncertainties in the assumptions, and a more robust and optimized feedback control modeling is needed. The variant, on the component side, requires the development of step-tuneable gyrotrons and, additionally, the development of broadband diamond window solutions, described in the next sections.

2.4. Reliability evaluations

The number of units to be installed in order to guarantee the prescribed system availability (to provide the required power for the specific tasks) depends on the gyrotron unit power, the reliability of all components and the transmission efficiency. The exact number to be installed, will depend on the actual reliability of the sources and the system components, on the availability of the parts during their lifetime according to the maintenance and replacement scheme and on the downtime in case of failure of a component. All these numbers have to be evaluated in detail when the system and components technology will be selected.

For dimensioning the EC system described in the following sections, some preliminary assumptions on the gyrotron and TL pulse reliability have been made. The design presently is assuming pulse reliability values for gyrotron sources, launcher and TLs of 98%, 99.9% and 99.9% respectively, with a power transmission efficiency of the TL of 85% and 2 MW power for each beamline at the output of the gyrotron. The assumption on gyrotron reliability is an extrapolation of the 95% reliability requirement for ITER gyrotrons [15] to the future 2 MW gyrotrons developed for DEMO. The higher reliability of launcher is assumed taking into account that the only movable part is the steerable mirror, while for the TL main failures in the cooling of mirrors can be prevented by redundancies in the circuits. These values have to be reconsidered once accurate estimates will be made. Pulse reliability is intended as the average fraction of pulses (2 h long) that are performed without failure by a subsystem.

In the preliminary analysis, summarized in [13] it is assumed for simplicity that the full pulse is lost if one malfunction occurs: in reality, in some cases the power (or part of the power) can be recovered some time after the fault occurs but still within pulse (e.g. the faulted gyrotron is restarted in a shorter time). In the analysis two additional risks are taken into account: the possibility that the power-per-unit at plasma is 10% less than expected for any reason (represented by 1.8 MW power at the source) and the possibility of having a failure that affects the capability of an entire port plug to be used, for example a fault on the main cooling system. The probability for the two cases is presently unknown, and they were computed separately, for several cases including some with 5–7 ports (launchers).

In order to provide the requested power ($30 + 30 + 70$ MW) for the different tasks with a mean-time between failure

(MTBF) of 10^4 (in average 1 failed pulses every 10 000 microwave pulses, corresponding to 1000 d of full-power operation), it is found that a total of 6 launchers powered by 12 clusters of 9 gyrotrons each (in total 108 gyrotrons) are needed. In case of the effective unit power of 1.8 MW the max failure rate of such a system would be 1 every 1000 pulses (100 d of operation), while in case of an accident causing the unavailability of one port the MTBF will drop to 175 pulses (17.5 d of operation).

At the moment, there is no defined requirement on the reliability of DEMO, still being conceived as an experimental device. As DEMO should survive all the events possibly leading to disruptions, where EC heating system acts a quick 'actuator' in the active control loop, especially for preventing disruptions as those expected in case of strong radiative instabilities, the EC system reliability must be very high.

3. Gyrotron design and developments

The microwave sources (gyrotrons) for DEMO are under development in the EU [16], both theoretically and experimentally, with the aim of increasing the output power per unit, the gyrotron efficiency, the robustness, the simplicity and the flexibility in operation, namely multi-purpose/multi-frequency operation and frequency step-tuneability.

3.1. Coaxial-cavity gyrotron development

Presently, the coaxial-cavity gyrotron technology is considered to be the most promising concept to reach multi-megawatt operation at frequencies equal or above 170 GHz. This is because the coaxial-cavity technology benefits from a reduced mode spectrum and a reduced voltage depression with respect to the conventional cylindrical cavity technology. An output power of 2 MW, a total gyrotron efficiency above 50% and the possible operation at multiple frequencies require significant developments in key components and technologies, together with the introduction of new gyrotron operating regimes. It includes the verification of advanced cooling concepts with the focus on the cavity cooling [17].

A major focus in the experimental work is the increase of the possible pulse length from 50 ms milliseconds up to one second of the KIT 2 MW modular-type coaxial-cavity pre-prototype. In parallel, a multi-frequency/multi-purpose short-pulse (ms) pre-prototype gyrotron is developed to demonstrate proper operation at 136/170/204/238 GHz. It bases on the existing 2 MW 170 GHz coaxial-cavity pre-prototype gyrotron (figure 1, left) [18]. For operation at different frequencies suitable operating modes are selected.

Key components, particularly, the magnetron injection gun (MIG), the coaxial cavity and the quasi-optical output coupler are to achieve an output power of about 2 MW and an interaction efficiency $> 35\%$ at 136 GHz, 170 GHz and 204 GHz, accordingly.

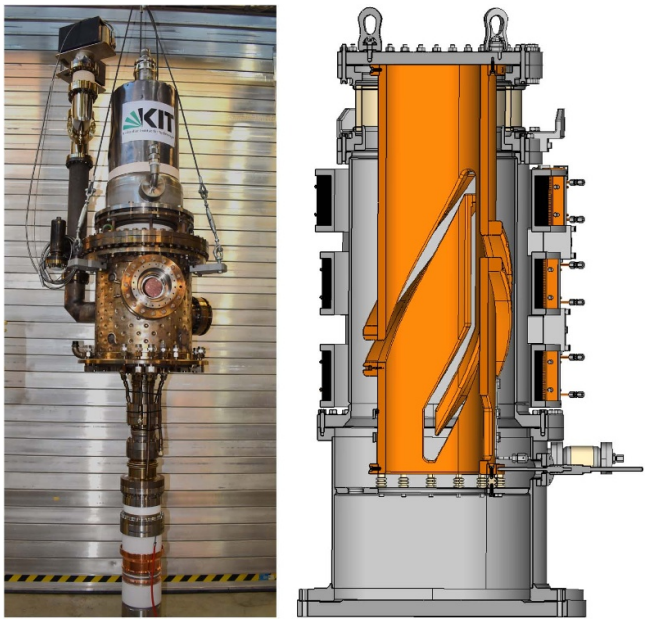

Figure 1. Left: the 2 MW 170 GHz coaxial-cavity longer-pulse pre-prototype gyrotron. Right: scheme of a prototype MDC.

3.2. Coaxial-cavity gyrotron testing

A test program on the modular coaxial-cavity gyrotron pre-prototype is ongoing at the new FULGOR gyrotron test facility at KIT, extending previous tests [19]. As already stated, the near-term target is to increase the pulse length of the modular type pre-prototype coaxial-cavity gyrotron up to 1 s. An update of the modular pre-prototype contains a CVD-diamond disk, a long-pulse collector and a new collector sweeping system. In parallel, experiments of the multi-purpose/multi-frequency and frequency step-tuneable operation [20] are prepared. As base for this experiments the quasi-optical output system, as one of the major gyrotron key components, is validated in cold measurements using a quasi-optical mode generator [21]. An excellent agreement between simulation and measurements has been demonstrated at all selected frequencies.

Experiments with the multi-frequency pre-prototype gyrotron will be performed at 136/170 GHz. The operation at 204 GHz and 238 GHz follow. Those experiments require the installation of the gyrotron into the new 10.5 T superconducting magnet.

3.3. Step-tuneable gyrotron studies

Step-tuneable gyrotrons for the TF variant are under development at EU. A tuning of the frequency by variation of the cavity magnetic field is considered to ensure a bandwidth of about ± 10 GHz [22].

The selected oscillation modes used for frequency tuning must fulfill three different criteria: (i) the mode eigenvalues have to correspond to the frequencies where the output window is transparent at a given cavity radius, (ii) a strong coupling of the modes to the electron beam has to be secured,

which is a criterion regarding MIG design and (iii) the modes need to have similar caustic radii $m/\chi_{m,n}$, which is a criterion regarding launcher design, where m is the azimuthal index, and $\chi_{m,n}$ is the mode eigenvalue [23]. In the case of a coaxial-cavity gyrotron, there is also a fourth criterion in which the thermal loading of the coaxial insert is a criterion during the mode selection process. An advanced mode series for frequency step-tuning is found. In total 11 modes are selected for each center frequency at 170 GHz and 204 GHz based on the 2 MW 170/204 GHz coaxial-cavity design [24]. Simulations indicate a possible output power of about 2 MW at 170 GHz and 204 GHz with a power deviation of around $\pm$ 8% over the whole frequency band.

Continuous magnetic field tuning is considered as an effective method for frequency step-tuning from upper to lower frequencies. However, it is found that this method cannot be used for tuning from lower to upper frequencies due to hysteresis effects [25]. In this case, the tuning methodology must consider to switch off the gyrotron shortly ($\sim$ 1 s [14]), to change the field of the superconducting magnet and to restart the gyrotron again.

3.4. Multi-stage depressed collector (MDC) studies

Work is ongoing to increase the efficiency above 50% by implementing a new MDC concept [26] which is based on the $E \times B$ drift. The idea is to separate the spent electrons according to their kinetic energy [27]. The design is based on minimum two electrodes that are separated by helical gaps to create azimuthal electric fields for radial electron drift [28, 29]. Slow and reflected electrons are collected at the first electrode with a low depression voltage while the majority of electrons with a high kinetic energy are collected at the second electrode with an increased depression voltage. Simulations show that a collector efficiency above 75% can be achieved. Considering 35% electron-beam efficiency it would correspond to a total gyrotron efficiency above 60 %.

The $E \times B$ MDC prototype developed at KIT (figure 1, right) shows a high flexibility and is compatible to different gyrotrons. It is possible to use the same collector for gyrotrons operating at various frequencies, even if considering second harmonic operation.

3.5. Theoretical and numerical studies

To secure stable and optimum gyrotron performance and to increase the operational margins, extensive theoretical and numerical studies have been ongoing, focusing on modeling, understanding, and suppression of unwanted parasitic oscillations. Such oscillations, when present, prevent the gyrotron from reaching the optimal high-power/high-efficiency operating regimes. Within those studies, the possibility of excitation of parasitic backward waves in the gyrotron cavity and spacer was, for the first time, demonstrated by multi-mode non-linear beam-wave interaction simulations [30]. Significant progress in the modeling and design of the gyrotron beam tunnel has also been achieved, concerning two different beam tunnel concepts for effective suppression of parasitic oscillations: the stacked, dielectric-loaded structure [31], currently used in European high-power gyrotrons [32], and a full-metallic structure bearing either random wall corrugations or a diffusive surface [33]. Experimental testing of the full-metallic beam tunnel concept has already been initiated [34].

4. TL up to the tokamak building

The design of the EC TL from the RF building to the tokamak is made considering the possibility to have access to the tokamak building at the sides of the assembly hall, with line paths running underground in tunnels partly below it (figure 2).

4.1. TL layout

The gyrotrons are located in two RF buildings at $\sim$140 m from the tokamak central axis to allow the properly gyrotron operations with any disturbances from the stray magnetic field of the tokamak. The TLs, all under vacuum, are partly realized with waveguides and partly by quasi-optical mirrors. In the RF and the tokamak buildings, corrugated waveguides are the preferred choice due to better management of safety, in particular for the tritium confinement in the tokamak building by means of RF windows and isolation valves. Outside the RF and the tokamak buildings, the beams of each cluster are transmitted jointly by a multi-beam (MB) quasi-optical TL similar to the one of Wendelstein 7-X (W7-X) [35] but evacuated down to 10^{-5} mbar as those planned for DTT [36, 37], to reduce maintenance, transmission losses and risk of arcs. The target power transmission efficiency of 85% includes the whole path from gyrotrons to the launcher. Each Multi-Beam Transmission Line (MBTL) is approximately 100 m long, where plane and parabolic mirrors alternate in a specific configuration. The complete layout is sketched in figure 2, where the MBTL connects the RF and the tokamak buildings, passing below the assembly hall.

The RF buildings, shown in figures 2 and 3, top, are such that the gyrotron cavities are placed at the height of the equatorial level of the tokamak, in order to minimize the radial component of the DEMO stray field, the most critical for the gyrotron performances. The placement at the DEMO equatorial level is consistent with the need to have a floor hosting the High Voltage Power Supplies (HVPS) just below. In fact, the HVPS of a gyrotron need to be placed close to the gyrotron, in order to minimize the length of the cables and their capacitance, to prevent gyrotron damages in case of internal arcs. An additional floor hosting the cooling circuits and other auxiliaries is conveniently put at the bottom.

The connection between waveguides and MBTL is obtained by suitable combining and splitting mirrors. The concepts developed for the TL in the different parts are detailed in the next subsections.

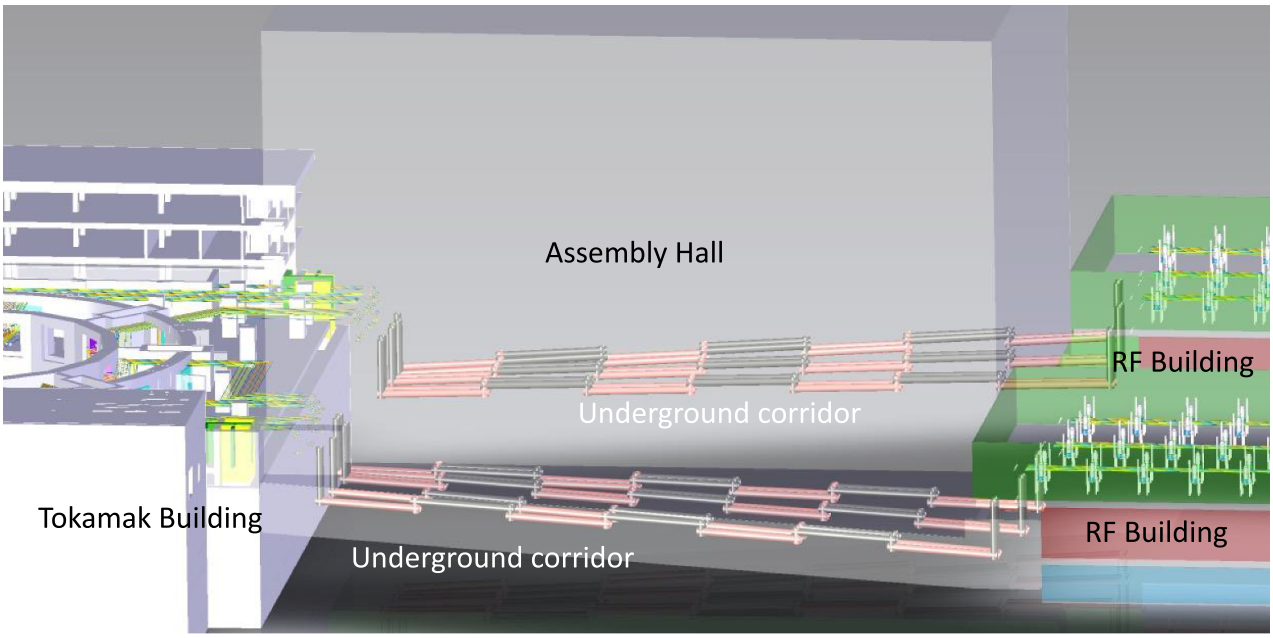

Figure 2. RF buildings (right) are linked to the tokamak hall (left) by the MBTL running in corridors under the assembly hall.

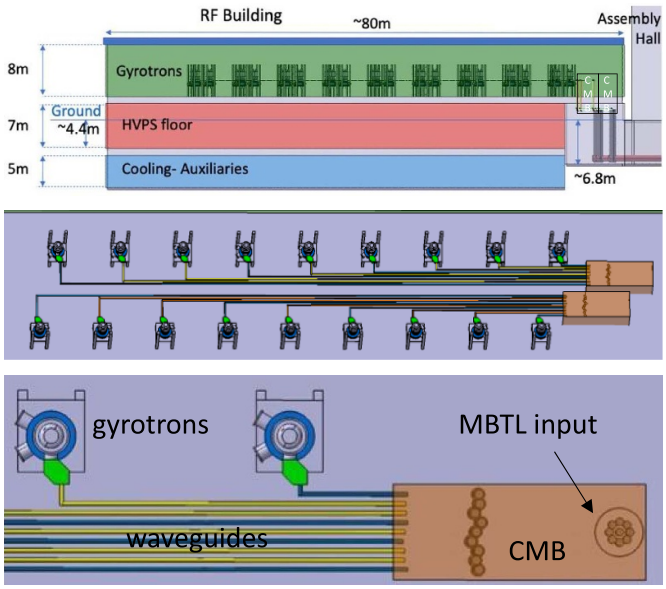

Figure 3. Top: side view of the RF building with required heights. Middle: view of the two facing rows of gyrotrons in the RF buildings with parallel waveguides and the MBTL connection at right. Bottom: detailed top view of two gyrotrons and the MBTL connection.

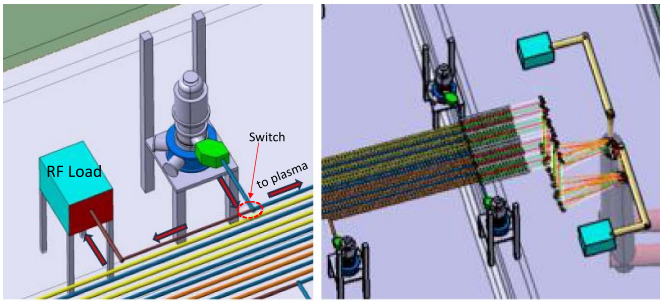

Figure 4. Two possible positioning for the calorimetric loads: close to each gyrotron (left) or shared by the gyrotron of each cluster (right).

4.2. TL in the RF building

The ideal cluster layout is the one shown in figure 3 top, with all gyrotrons in a row and all outputs facing the same side (in direction perpendicular to the line).

The gyrotrons launch power into circularly corrugated HE_{11} waveguides horizontally placed, with miter bends deviating the beams at 90 deg in such a way to realize an array of parallel waveguides with axes at a distance of around 200 mm between each other (figure 3(bottom)). A second cluster with gyrotron output facing the output of the first cluster, allows the pairing of two MBTL running close to each other as convenient for the routing. The reference waveguide inner diameter is 63.5 mm, for carrying up to 2 MW.

Gyrotrons are placed with their axes at a distance of 6 m between each other, to avoid the mutual interferences of the magnetic fields. If the polarization at the gyrotron output is horizontal, the path guarantees that it is kept close to horizontal also in the MBTL.

Calorimetric loads for gyrotron conditioning could be placed close to each gyrotron and connected with a switch (figure 4, left) or shared by each gyrotron of a cluster (figure 4, right). In this last case the beams are directed (one at a time) precisely by movable mirrors to a quasi-optical dedicated line guiding the beams to the matched load.

Both solutions can be convenient depending on the strategy for gyrotron conditioning and recovery from a fault (e.g. after an internal arc).

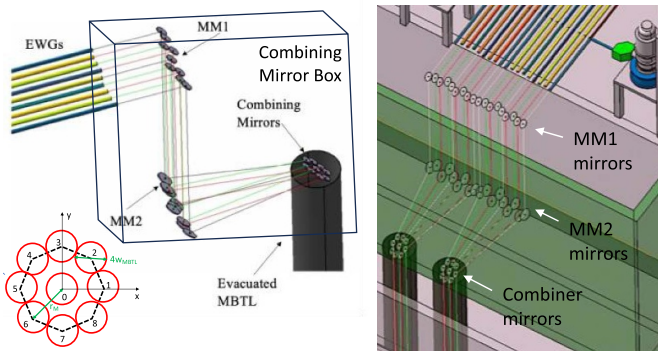

Figure 5. Detailed views of the CMB with the matching mirrors MM1, MM2 and the combiners.

4.3. Coupling to the MBTL

The coupling of the waveguide bundle to the MBTL is realized with a mirror system in the Combining Mirror Box (CMB) under vacuum. The Gaussian beams, output from the waveguide with optimal waist radius w_g, are matched to the ones with ideal waist radius w_M for the MBTL with two mirrors MM1 and MM2 with focals f_1 and f_2, in confocal 'telescope' arrangement (figure 5). The matching is obtained choosing f_1 and f_2, in a ratio equal to the ratio of beam waist size, $f_1/f_2 = w_g/w_M$ and placing the mirror MM1 at f_1 from the waveguide aperture, MM2 at $f_1 + f_2$ from MM1 and the position of the combiner at f_2. The matching is effective for beams at all frequencies. Plane 'combiner' mirrors are placed in the proximity of the entrance of the MBTL, close to the beam waist (minimum) position and packed closely for all the lines of the cluster. The set of combiners couples all the beams of the cluster into a single bundle with parallel axes in a symmetric arrangement (at the vertexes and in the center of an octagon, as shown in figure 5). The alignment of beams is done mainly by angular movements. Typical alignment accuracy required for the optics is ± 0.5 mrad. The mirrors MM2 are movable between two fixed positions, to provide the deviation of the beam to the quasi-optical line to the load in the option of figure 4, right.

4.4. Quasi-optical MBTL layout

The power of a cluster is transmitted by a MBTL as shown figure 6: it consists of a MB bundle (one bundle with all the beams of a cluster) guided by mirrors at regular distances to form quasi-optical TLs and enclosed by pipes extending from the RF building to the tokamak building. The beam transmission with the maximum efficiency can be realized by a set of Focusing (FM) and Plane (PM) mirrors, in a specific confocal setup, as will be explained below. The line starts with the bundle of beams directed from the CMB downward to a first MB focusing mirror (FM1), at the level of an underground corridor below the DEMO assembly hall. The mirrors are placed at regular distances in a straight path and the last mirror of the MBTL, FM8, directs the beams upward, to the Splitting Mirror Box (SMB) and the EWGs placed at the equatorial level of the DEMO (figure 6).

4.5. Quasi-optical MBTL concept and design

The chosen specific confocal mirror setup has been demonstrated to transmit power with minimal losses in the TL of W7-X [35]. It can be shown that natural deformations of pure TEM_{00} (Gaussian) beams due to off-axis reflection deformations, described in [38], can be partially compensated in a confocal optical system when the number of focusing mirrors is a multiple of four, provided a specific arrangement of the mirrors reflecting surfaces is used (square configuration, see [39]). Confocal means that the focusing mirror distance is twice the mirror focal length f_M. Such a layout, is capable to transmit with very low deformation a set of beams properly spaced, which share the same mirrors, thus minimizing the number of mirrors and the mirror area required for the TL.

The beams between two FMs propagate alternating crossing or parallel paths. On the FMs they are partially superimposed with well separated centers, and beams have the maximum size, thus the lower power density. On the PMs, being close to the FMs, the maximum power density is slightly higher due to the smaller dimension of the beam spots, but still well manageable.

The MBTL mirrors are designed large enough to intercept 99.9% of the power at the lowest frequency (136 GHz). The mirror spacing and the beam waist dimension in the MBTL section were studied to provide a manageable mirror size and a sufficiently long run to cover the tunnel length ($\sim$100 m) for all the clusters. The minimum radial dimension of FMs is chosen on the basis of the space needed for the bundle of beams propagating from the waist location close to the CM (where they have to be individually injected in parallel) up to the FM where they should be reflected. The envelope considered for defining the mirror size is the one containing all the beam contours at radii $2r_M$ where r_M is the radius at $1/e$ of the peak field amplitude of each beam at a distance f_M i.e. at the FM.

Calculations for the minimal mirror radial dimension as a function of beam waist for the two options with 4 (larger) and 8 (smaller) FMs have been made, and, while the choice of larger mirrors corresponds to halved ohmic losses due to less reflections, they require more than doubled enclosure volumes ($\sim$180 vs. 80 m^3) with larger inner surface to pump and less manageable mirror sizes. The preferred choice for the MBTL is then a line with 8 FMs. The chosen MBTL consists in this case of eight parabolic mirrors and six plane mirrors, as shown in figure 6.

4.6. Quasi-optical MBTL modeling

The transmission of Gaussian beams from the combiner to the splitter has been modeled with the electromagnetic code GRASP [40] for the ideal parabolic mirror surface and the lowest frequency (136 GHz). A first evaluation of the spillover and the coupling losses have been obtained in the ideal case of aligned and undeformed mirrors and ideal input Gaussian beams. The GRASP model implemented so far has input at the combiners and output at the splitter, where the beams are parallel. The FM surfaces are modeled as off-axis parabolas with

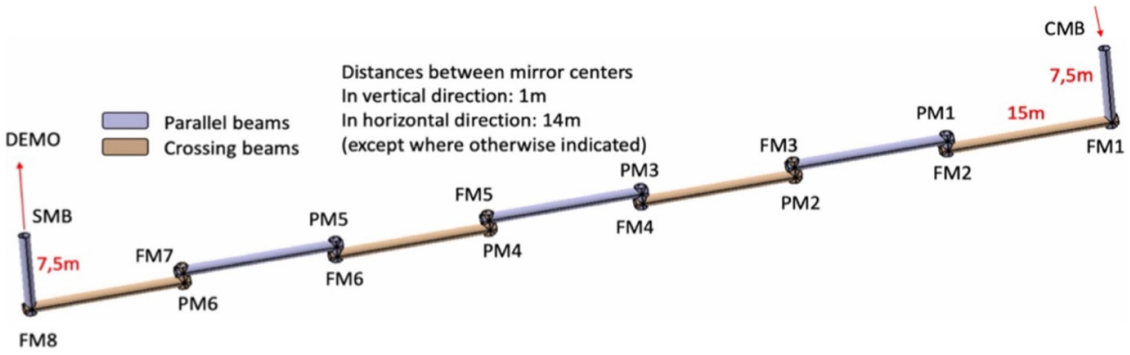

Figure 6. The MBTL for one cluster consists of eight focusing mirrors (FM1-8) and six plane mirrors (PM1-6).

focus at a distance f_M from the mirror center. They result at the intersections of beam axes. With the code, the power lost from the TL being not intercepted by all mirrors (spillover loss) and the power not found in the nominal TEM_{00} mode at the output (coupling loss) can be computed for each beam separately. The spillover loss found for the sequence of 8 FMs and 6 PMs is very low: in average around 0.038%. We note that the central beam, as expected, has negligible spillover loss.

The coupling losses, due to the non-ideality of the beam reflections and their trajectories with respect to the mirror centers were computed in the ideal case of aligned and undeformed mirrors. The coupling refers to the power fraction remaining in the fundamental Gaussian beam centered around the propagated beam axis on the exit plane where the beam waists are expected. The coupling loss is somewhat a measure of the deformation of the beam along the TL: it does not mean that the power is not transmitted. For example, if the coupling loss consists in a small deviation of the beam at the end of the MBTL, it can be partially recovered by aligning the matching mirrors in the SMB. From the computed results, the fraction of power lost to the TEM_{00} mode in the MBTL is in average less than 0.1%.

At the end of the MBTL the beams are found in the expected position, numbered from B0 (at center) to B8 (figure 7, top). In figure 7 (center and bottom) the pattern of radiation at the exit of the MBTL in the ideal undeformed mirror case is shown. The evaluation is done at the minimum frequency of 136 GHz, the one subject to higher truncation losses on the mirrors.

4.7. Estimate of MBTL ohmic losses

A first estimate of the ohmic losses in the MBTL can be made on the basis of the number of the mirrors and the polarization incident on them. For mirrors, pure copper with resistivity 1.74 $\mu\Omega$cm, corresponding to a temperature of $\sim$30 °C [41] is assumed, with a multiplicative (roughness) factor of 1.3 [42].

An average of the ohmic losses in the MBTL, taking into account all (20) mirrors including input/output single beam optics, excluding polarizers and waveguides is 2.0% (2.2%, 2.4%) for the frequencies 136 (170, 204) GHz. The losses expected for two polarizers are 0.80%, (0.90%, 1.0%), while for the TL the losses expected for ideal alignment are of the order of 3% including miter bends at all frequencies. Total expected ohmic losses are around 6%–6.5%. Due to the long pulse of DEMO (2 h) all the mirrors and waveguides have to be actively cooled. A single cooling system for all elements of one cluster is envisaged. So far, thermal simulations have been performed only for the MBTL mirrors, as seen in the next section.

4.8. MBTL mirrors

A first design of the mirror structure and the cooling circuit for the large mirror has been realized (figure 8, top). The mirror has a honeycomb AISI 316 l steel structure 60 mm thick, the surface dug with a Cooling Channel (CC) with a spiral shape and a semi-circular section and a pure copper surface layer with a thickness of 2 mm. The honeycomb allows to lower the weight ($\sim$210 kg) by 57% with respect to a bulky mirror of the same size and the maximum deformation to 0.05 mm (50% less with respect to a thinner mirror of the same weight). The copper layer can be deposited on top by electrodeposition and then machined to the desired shape.

Thermal simulations in steady state (given the pulse length of 2 h) were performed with the ANSYS suite, for the expected losses for a 2 MW beam at 204 GHz (highest thermal load and minimum spot size among the used frequencies) and a cooling water at 15 °C input (tentative value), with volume flow rate of 60 l min^{-1}, to extract the absorbed power of 20.9 kW. Temperature and thermal deformation maps are obtained, showing a maximum temperature less than 30 °C (figure 8, bottom), and combined thermal and gravity maximum deformation lower than 0.07 mm.

The deformed surface maps are used to analyze the beam quality degradation along the line due to mirror deformations and then optimize the cooling to minimize the power losses. A first design of the mounting structures is shown in figure 9, left.

4.9. Splitting mirrors and polarizers

The Gaussian beams will exit from the MBTL parallel and with waist location on a plane. A set of plane splitting mirrors close to the beam waist location but at three different heights

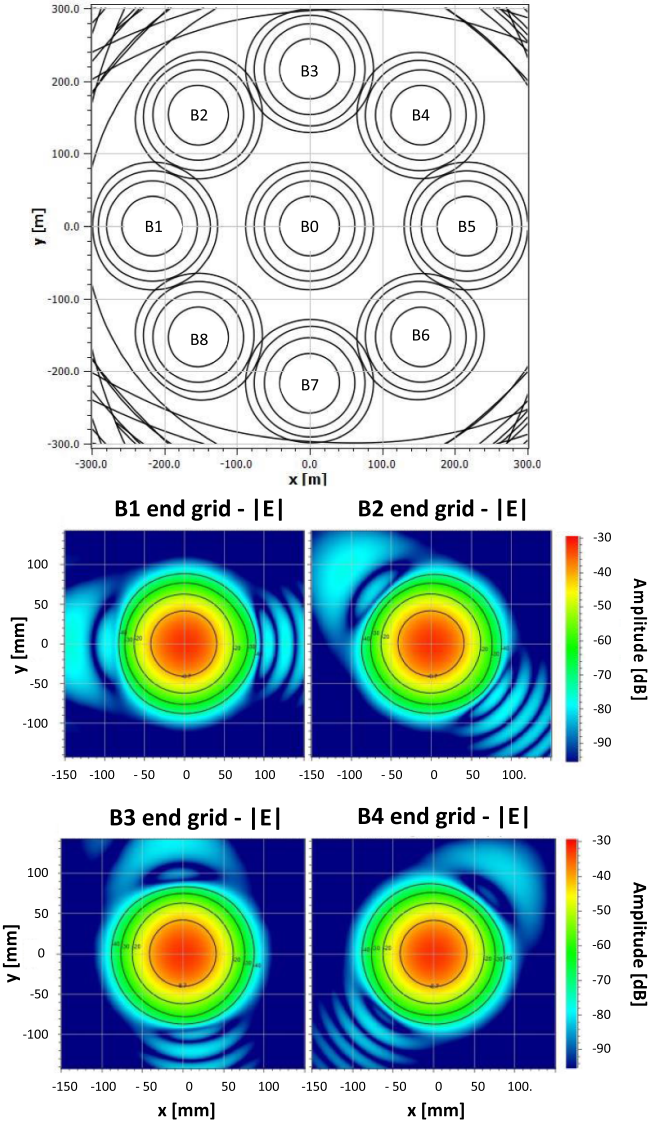

Figure 7. Top: patterns of radiation on a plane grid at the exit of the MBTL, in the ideal case of aligned and undeformed mirrors and ideal input Gaussian beams. Amplitude field patterns in dB (arbitrary scale) are shown for beams B1 to B4 (middle and bottom), while beams from B5 to B8 have corresponding patterns, due to the symmetry. Field contours are shown by solid lines at −8.7, −20, −30, −40 dB with respect to the peak power.

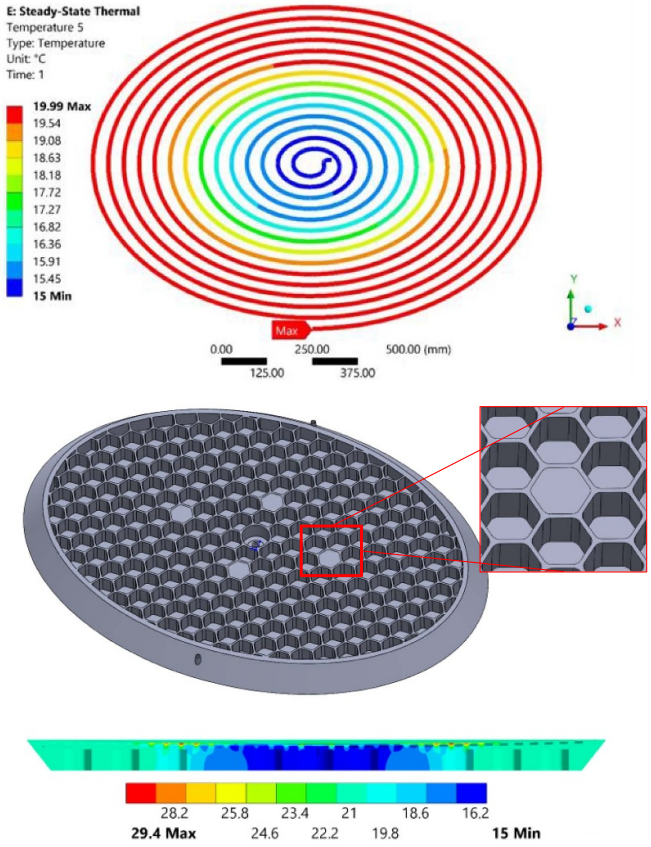

Figure 8. Focusing mirror modeling: Top: shape of the spiral channel and water temperature evaluation in steady-state. Middle: honeycomb structure on the back side. Bottom: section with temperature map calculations (units in °C).

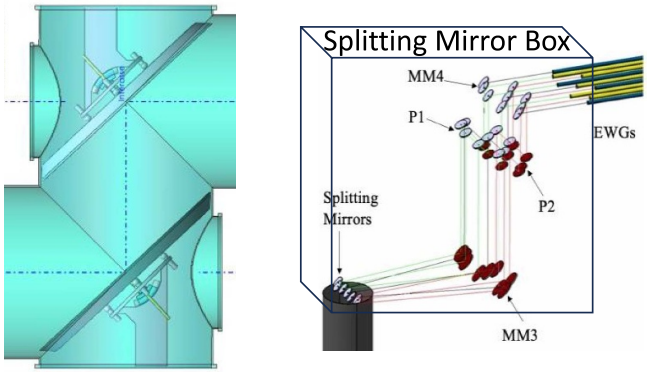

Figure 9. Left: MBTL mirrors on the mountings in the enclosure. Right: the SMB including mirrors and polarizers.

separate the beams and direct them onto a couple of matching mirrors (MM3 and MM4) very similar to the MM2 and MM1 (figure 9, right).

The ratio of the focals of MM3 and MM4 f_4/f_3 must be equal to w_g/w_M in order to match the beams to the bundle of corrugated waveguides at the exit of the SMB.

In addition, a couple of grooved polarizing mirrors P1 and P2 are inserted in the vertical section of the line, close to the beam waist between MM3 and MM4, to allow the selection of the polarization of the wave launched into the plasma.

Broadband polarizing mirrors have been studied for inclusion in the quasi-optical path, to be used for at least two different frequencies (136–170 GHz and 170–204 GHz ranges were investigated). To exhibit the lowest ohmic losses and provide any arbitrary output polarization also at higher frequencies (up to 204 GHz) the two polarizing mirrors have identical groove depth corresponding to $\lambda_0/8$, where λ_0 is the free-space wavelength at the lowest frequency (136 GHz) of the DEMO EC system. A numerical model is used for the calculation of the polarization of the output beam for each frequency and the selection of the mirror rotation angle solution providing the lowest possible ohmic losses at the polarizers (figure 10) [43].

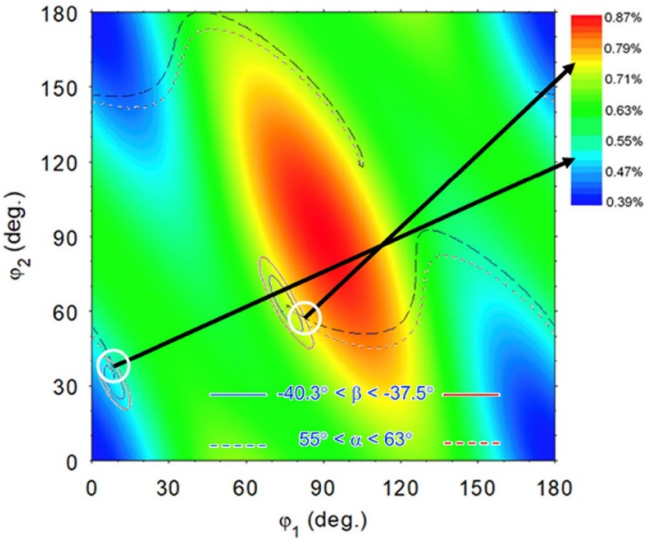

Figure 10. Calculated ohmic losses for two polarizers as a function of their rotation angles ϕ_1 and ϕ_2. The angular ranges providing a specific polarization for a specific O-mode injection are indicated by the white circles.

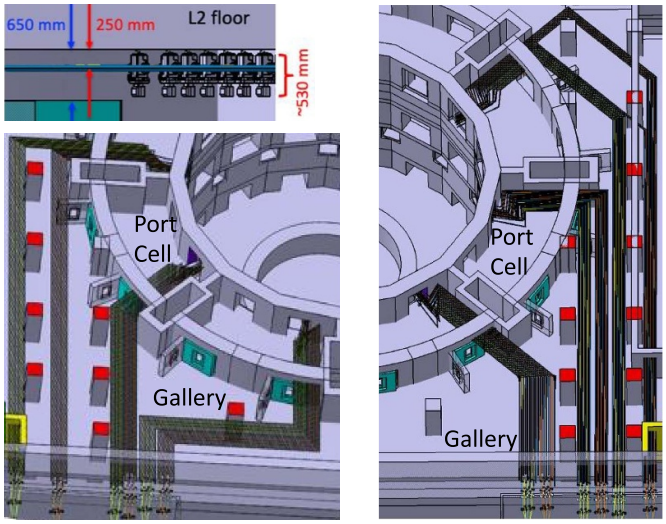

Figure 11. Top left: side view of the lines running close to the ceiling of the equatorial level. Bottom left: EWG routing to ports 8, 10 and 12. Right, EWG routing to ports 14, 16 and 2.

5. TL in the tokamak building

In the tokamak building, corrugated waveguides are the preferred choice due to a higher safety, in particular for the tritium confinement, with the possibility of isolation of single lines with multiple isolation valves, essential in case of faults of components as RF windows, and preventing the contamination of the TL outside the tokamak building.

5.1. TL layout in the tokamak building

The routing of the EWGs in the tokamak building has been defined (figure 11).

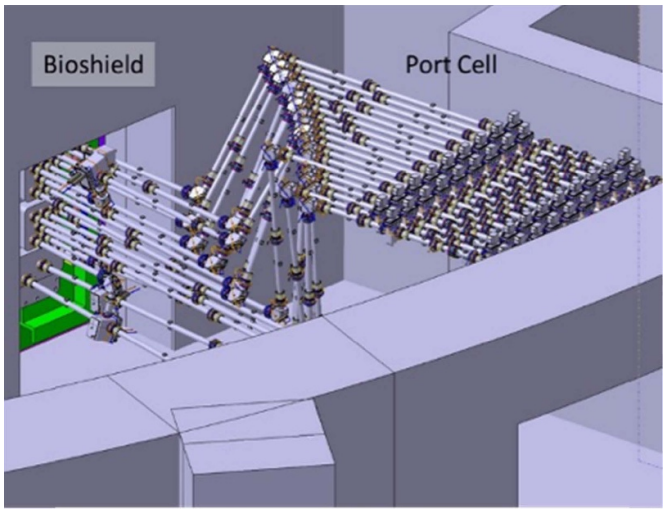

Figure 12. EWG routing and components in the Port Cell.

In the Port Cells (PCs) the TL routing is kept identical for all ports: the differences are limited to the gallery, where the routing to the ports dedicated to the EC system (even ports 8–16 and port 2 are chosen for convenience) has been studied to reach the south wall of tokamak building with the lowest number of miter-bends, using, when possible, the miter-bend angle of 90 deg. The EWGs run in the gallery close to the ceiling of level 1 of the tokamak building with a distance of ∼200 mm among the EWGs axes; the routing is compatible with the fixed positions of the pillars in the gallery (figure 11). The layout in the PC is shown in figure 12.

5.2. TL components

The design of the evacuated components for primary vacuum is under way, as well as their integration in the PC (figure 12) [44]: parametric models are set, allowing change for the main parameters, considering double confinement between the interior and the outer space and providing cooling and a vacuum monitoring on the interspace between the two seals.

The design of two basic components is shown in figure 13. To reduce the weight and space requirements of each component for Remote Handling (RH) purposes, the design includes CCs embedded directly within the thickness of the component. These CCs are created by drilling deep holes throughout the component, situated between the inner and outer walls of the component. Additionally, to minimize tritium permeation through the EWG wall, a design was investigated, using two coaxial layers of CCs that are angularly offset to extend the tritium diffusion path through the EWG wall. A joint work with the DEMO RH team has been started to define the space requirements for RH tools and the best design option for the maintainability of the components.

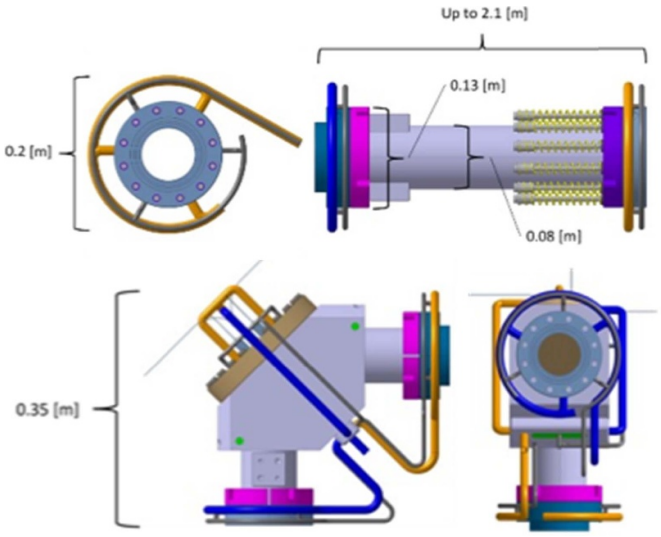

Figure 13. Top: model for a single straight EWG. Bottom: miter bend.

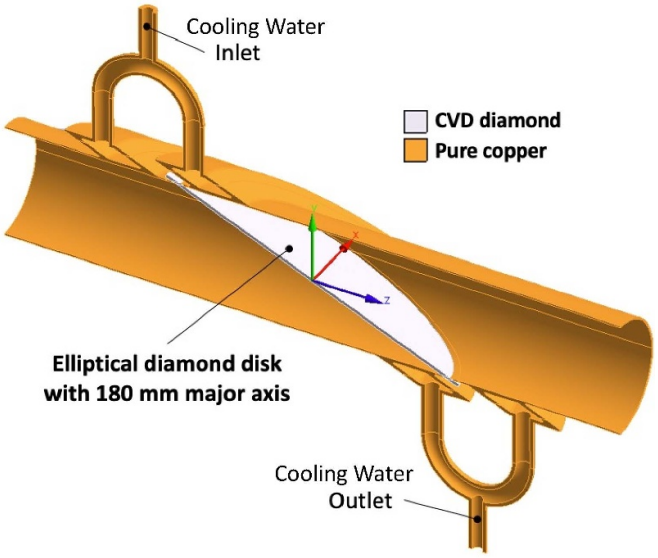

Figure 14. Geometry of the Brewster-angle diamond window featuring the large diamond disk.

5.3. Diamond vacuum window

A major challenge is the diamond vacuum window: in particular the TF variant needs broadband solutions like the Brewster-angle and double-disk diamond windows and polarizing miter bends in the primary vacuum.

The TF represents a design option to investigate: it would simplify the port plug integration (no actuators and moveable components including their cooling system) and their maintenance, with consequent improvement of reliability and lifetime. In the TF variant of the EC system, Brewster-angle windows can be mounted both at torus and gyrotron locations.

The Brewster-angle window represents the primary choice thanks to its intrinsic simplicity, although feasibility of manufacturing of Brewster-angle large diamond disk windows is still to be checked and polarizers are in this case required on the torus side of the window. It is shown in figure 14. The diamond disk is inclined at the Brewster angle of 67.2° for diamond and the feasibility of this window concept was successfully shown in a MW-class, D-band, tuneable gyrotron prototype, but only for short pulses and a 50 mm aperture [45]. The 2 MW wave propagation requires a minimum aperture of 63.5 mm, which imposes a diamond disk with a minimum diameter of 180 mm, well beyond the current technological limits (∼140 mm) of the Microwave Plasma-Assisted (MPA) reactors where these disks are usually grown.

In the last years, the challenging target of a Ø180 mm disk with a thickness of about 2.0 mm has been faced with extensive diamond growth experiments performed by the industrial partner Diamond Materials GmbH in Freiburg, Germany [46] and related loss tangent measurements at KIT. This led to the worldwide first free-standing optical grade diamond disk with Ø180 mm and average unpolished thickness of about 1.3 mm [47].

The performance of the Brewster-angle window featuring these large diamond disks was also characterized by a consistent and parametric analysis work in view of the forthcoming window prototyping activity. Computational fluid dynamics (CFDs) conjugated heat transfer analyses were carried out to check the water behavior and the thermal performance of the window with respect to the worst beam scenario of 2 MW at 204 GHz.

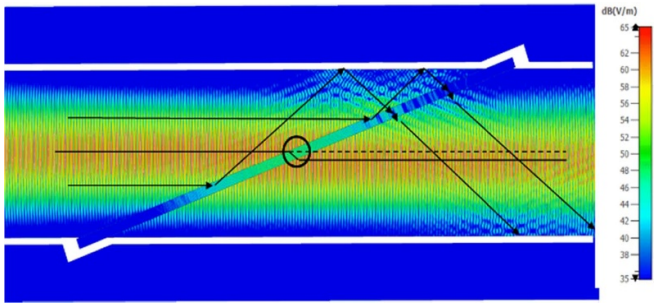

Figure 15. Simulated electric field distribution in a Brewster window with the incident Gaussian beam from the left and reflection directions indicated by arrows.

The resulting temperature distributions were subsequently transferred to structural analyses, taking also into account other operational loads like gravity and coolant pressure, to validate the design against the allowable limits. Temperatures and stresses in the window are well below the limits.

The electromagnetic modeling of the window is currently under development. In figure 15 the simulated electric field distribution is shown, with evidences of possible reflections effects at the waveguide walls and in the diamond disk.

Prototyping and testing activities can be implemented to show the manufacturing feasibility of such a window for long pulse gyrotron tuneable operation in MW-class. Besides the large disk, a major challenge is the asymmetric brazing joint between diamond and copper of a very large disk.

For the TF system the Brewster-angle gyrotron window is a physically simple solution for the linear polarized output

beam. In the case of showstoppers, the double-disk diamond window represents the backup solution. This concept was used at ASDEX upgrade for injection of up to 1 MW at four frequencies between 105 and 140 GHz [48].

For the torus window, part of the first confinement system, the tuneable double-disk diamond window has two advantages over the Brewster-angle window: on one side a better mechanical confinement protection by two diamond disks and on the other side no polarization dependency. This window was investigated by CFD conjugated heat transfer and structural analyses to check its performance within the DEMO boundary conditions [49]. The sensitivity of the design with respect to various parameters like mass flow rate, loss tangent, beam radius and frequency was checked.

Temperature and thermal stress results showed that the double-disk diamond window is a feasible window solution for DEMO, but safety margins against limits shall be increased by introducing design features able to make water more turbulent in the cooling path.

6. EC launcher design

The launcher design is driven by the power and deposition location requirements for the different tasks given to the EC system: 30 MW for BH deposited in the plasma center, 30 MW in narrow beams at the location of the 2:1 and 3:2 NTM instabilities, and additional 70 MW at the plasma edge in case of tungsten impurity influx, for RI suppression (table 1).

6.1. Concept of a modular launcher

The launcher, including fixed mirrors, shielding blocks and launching waveguides, is made in two parts: on one side the launching mirror antennas, on the opposite the fixed mirrors and the input waveguides.

The need of narrow beams at the resonance for the NTM require large mirrors to focus the beams, and thus specialized antennas, while the central and edge heating can be obtained with a unified nearly-equatorial launch, injecting different frequencies resonating at center or close to the edge, with smaller antennas hosting a larger number of beams.

In the concept developed so far, a launcher consists of 4 modules (antennas), aligned vertically from top to bottom, capable of launching respectively 3, 8, 8, 3 beams (22 beamlines, figure 16).

The launching mirror block, being exposed to the plasma and subject to radiation damages, can be extracted and replaced leaving the fixed mirrors block, the internal shielding blocks and waveguides in place, easing the maintenance of the most critical parts [50]. The basic steps of launching mirror module extraction for (remote) maintenance (figure 17) are:

- Open closure plate subplate (1).
- Cut supply lines (2).
- Loosen fasteners (3).
- Approach RM manipulator, connect with the launching mirror module and remove it (4).

The module extraction can be guided by rails at the bottom of the port plug (in yellow in figure 17).

All the modules at the right of the port can be left in place during the launching mirror module extraction. They also can be removed in case of fault, by removing the external and internal waveguides, opening the closure plate, extracting the shielding modules and finally the fixed mirror module.

6.2. Launching antennas

The beams on the top and bottom antennas (movable in the FF, fixed in the TF variants) are used for NTMs control at 170 GHz.

Being the antennas closer to the deposition location and the trajectory tangential to the flux surfaces, the plasma refraction effects and the tilt angle required for the aiming at the rational surface are minimized.

Having found a higher current-drive efficiency for injection at the lower side, the lower NTM antenna is aiming at the $q = 2{:}1$ surface, the NTM instability there requiring more power, while the top NTM antenna is aiming at the $q = 3{:}2$ surface (figure 18, left).

In figure 18 the beam trajectories for the nominal and extreme position of the steerable mirrors range are shown, together with the cold EC resonance (in orange) and the rational $q = 3{:}2$ and $q = 2{:}1$ surfaces (in green, dashed-dotted lines). The BH and RI beams share two symmetric modules (antennas) close to the equatorial plane with 8 beams each, that travel partially superimposed in the launcher and are refocused at the plasma side in order to require the minimum aperture on the BB.

The two central launching mirrors are fixed: a different resonant frequency is used to inject power in the plasma center (170/204 GHz) (see figure 18, right for beam-tracing at 170 GHz) or at the edge (136 GHz). Extensive beam-tracing analyses have been performed to define launching angles.

The optics of the NTM antennas is studied to have the three beams equivalent in toroidal symmetry when in the nominal position, resulting in equal trajectories and equal deposition profiles independently on plasma shape and refraction in an axisymmetric plasma. The optics for the BH/RI mirrors have been studied to have a moderate focusing and the beam bundle section as low as possible in the BB opening.

6.3. Mirror steering mechanism

For the FF variant a mirror steering mechanism is required, placed behind the mirror for radiation protection, while keeping the mirror rotation axis on the mirror surface, thus avoiding the need of a bigger mirror and a partial degradation of the optical performance with a different rotation axis. It is realized with an innovative pantograph structure, shown in figure 19, and is moved by pneumatic (bellow) actuators.

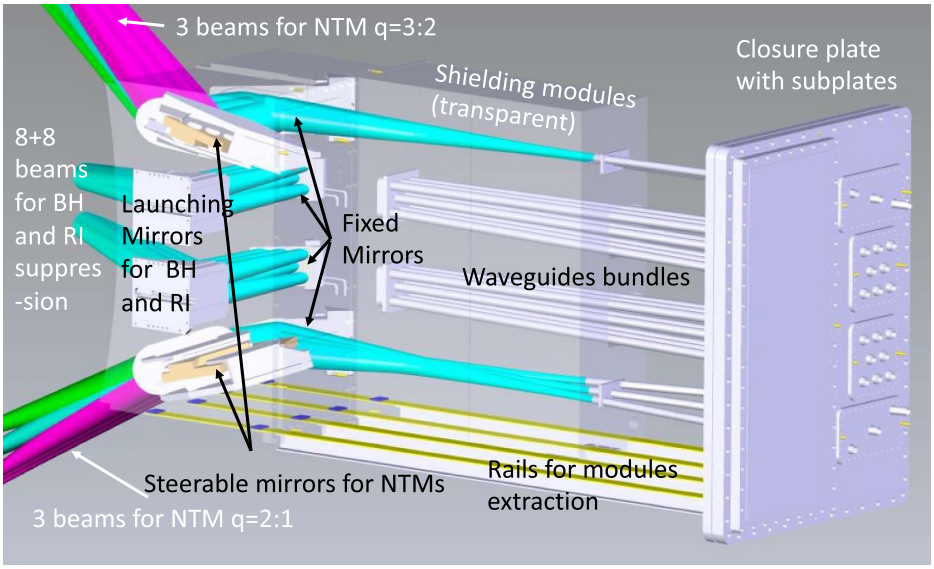

Figure 16. Launcher main parts and beam trajectories at 170 GHz (in color for three different positions of the NTM mirrors).

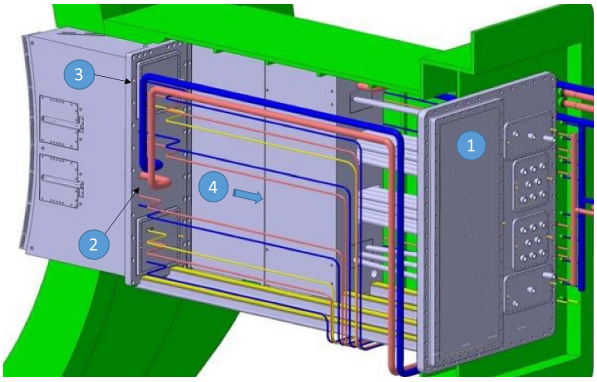

Figure 17. Basic steps of steering mirror module removal for remote maintenance.

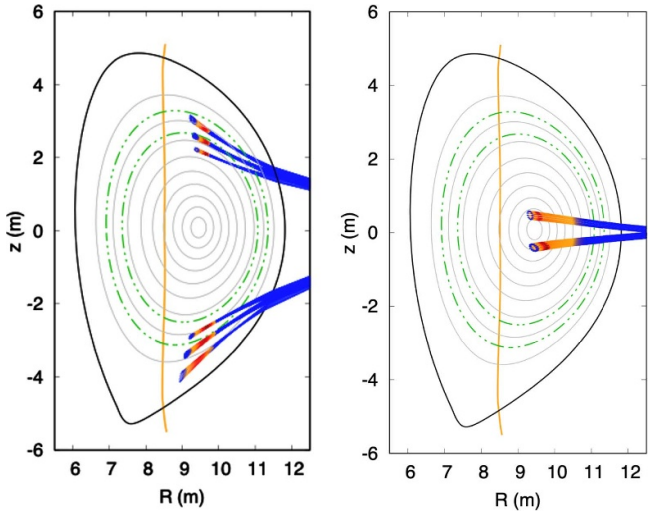

Figure 18. Left: beam tracing trajectories aiming at 2:1 and 3:2 NTM locations (dashed-dotted lines) for the nominal and extreme position of the steerable mirrors range. Right: beams aiming at the plasma center.

6.4. Launcher mirrors design

The design of the mirror structures, supports and cooling is addressed, checking temperatures and stresses. Several mirror cooling concepts are being studied: the main challenges for cooling are the higher power density released by the eight beams in the BH modules, where the beams footprints are smaller, and the temperature uniformity, to be maintained also in the support, to lower the stresses in the joining regions.

The mirrors inside the launcher consist of a plane reflecting surface made of CuCrZr and a 316 l(N)-IG support. Their water-CCs are designed to withstand the neutronic heating and the ohmic losses generated by the mm-wave beams [51]. In the case of the NTM antenna (figure 20(*a*)), the neutronic heating is the dominant thermal load, whereas for the BH mirrors (figures 20(*b*)–(*d*)) the main heat load is the ohmic loss.

Therefore, different cooling strategies were applied for each mirror: in the mirrors for NTM, the CCs are distributed in the whole volume, while in the BH mirrors all the flow is focused on reducing the temperature and the thermal gradient in the reflecting surface.

The design in most of the cases gives satisfactory values in terms of pressure drop and deformation, as well as temperatures below 350 °C, the limit of the materials (see figures 20(*a*) and (*b*)).

For the BH mirror facing the plasma the plasma radiation is considered as a uniform surface load of 40 kW m^{-2} applied on the reflective surface of the mirror. The highest peak load is found in the beam spots, reaching the value of 2 MW m^{-2}. The use of V-ribbed parallel CCs, as those actually foreseen for the first wall of the DEMO Helium-Cooled Pebble-Bed BB, has been considered.

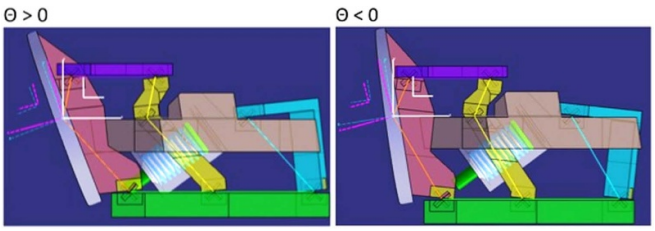

Figure 19. Sketch of the steering mechanism rotating the mirror surface at two different angles $\Theta > 0$ and $\Theta < 0$ around a virtual axis on the mirror surface.

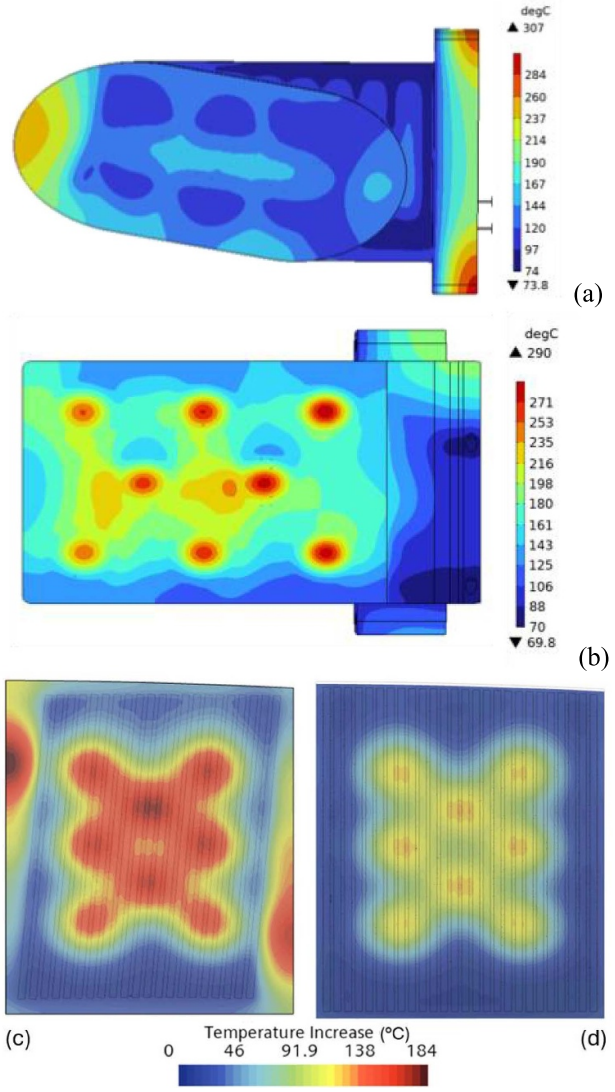

Figure 20. (*a*) NTM mirror temperature map. (*b*) Temperature map for the BH mirror not exposed to plasma. (*c*) Temperature increase for the BH mirror exposed to plasma in case of cooling with 21 smooth channels and (*d*) 26 ribbed channels in parallel.

That kind of turbulence promoters has been demonstrated to give very good results even when flow rate of 200 l min^{-1} of subcooled water at 5 MPa, 130 °C is used as coolant. With respect to smooth channels (figure 20(*c*)) the hot spot temperature of the surface decreases by 30%, as shown in figure 20(*d*), with a pressure drop below 2.5 bar.

7. Conclusions

The work on the conceptual design of the DEMO EC system is progressing with studies addressing the main challenges: the high-power generation with efficiency and reliability, the power transmission with minimal losses and good beam quality, the installation of complex components in a restricted space with RH, and the design of mirrors with high power density, requiring materials resistant to irradiation damage and replacement.

Acknowledgments

This work has been carried out within the framework of the EUROfusion Consortium, partially funded by the European Union via the Euratom Research and Training Programme (Grant Agreement No 101052200—EUROfusion). The Swiss contribution to this work has been funded by the Swiss State Secretariat for Education, Research and Innovation (SERI). Views and opinions expressed are however those of the author(s) only and do not necessarily reflect those of the European Union, the European Commission or SERI. Neither the European Union nor the European Commission nor SERI can be held responsible for them.

ORCID iDs

Alessandro Bruschi https://orcid.org/0000-0002-0139-6401
Chuanren Wu https://orcid.org/0000-0002-2523-1476
Kostas Avramidis https://orcid.org/0000-0001-9493-0468
Benedetta Baiocchi https://orcid.org/0000-0002-1483-3113
Ioannis Chelis https://orcid.org/0000-0003-2997-2586
Lorenzo Figini https://orcid.org/0000-0002-0034-4028
Timothy P. Goodman https://orcid.org/0000-0002-2464-6303
Zisis Ioannidis https://orcid.org/0000-0002-1233-9111
Alessandra Salvitti https://orcid.org/0000-0002-0195-758X
Laura Savoldi https://orcid.org/0000-0002-0267-2877
Christos Tsironis https://orcid.org/0000-0002-5212-7359

References

[1] Donné A.J.H. *et al* 2018 *European Research Roadmap to the Realisation of Fusion Energy*
[2] Federici G., Holden J., Baylard C. and Beaumont A. 2021 *Fusion Eng. Des.* **173** 112959
[3] Federici G. *et al* 2019 *Nucl. Fusion* **59** 066013
[4] Siccinio M. *et al* 2022 *Fusion Eng. Des.* **179** 113123
[5] Tran M.Q.T. *et al* 2022 *Fusion Eng. Des.* **180** 113159
[6] Garavaglia S. *et al* 2020 *Fusion Eng. Des.* **156** 111594
[7] Siccinio M., Graves J.P., Kembleton R., Lux H., Maviglia F., Morris A.W., Morris J. and Zohm H. 2022 *Fusion Eng. Des.* **176** 113047
[8] Kasparek W., Gantenbein G., Plaum B., Wacker R., Chirkov A.V., Denisov G.G., Kuzikov S.V., Ohkubo K., Hollmann F. and Wagner D. 2003 *Nucl. Fusion* **43** 1505

[9] Moro A., Bruschi A., Franke T., Garavaglia S., Granucci G., Grossetti G., Hizanidis K., Tigelis I., Tran M.-Q. and Tsironis C. 2017 *EPJ Web Conf.* **157** 03036
[10] Granucci G. *et al* 2017 *Nucl. Fusion* **57** 116009
[11] Cufar A., Bruschi A., Fischer U., Franke T., Granucci G., Grossetti G., Kodeli I.A., Trombetta D. and Villari R. 2019 *Fusion Eng. Des.* **146** 336–40
[12] Granucci G. *et al* 2017 *EPJ Web Conf.* **149** 03003
[13] Franke T. *et al* 2021 *Fusion Eng. Des.* **168** 112653
[14] Wu C. *et al* 2021 *Fusion Eng. Des.* **173** 112931
[15] Thumm M.K.A., Denisov G.G., Sakamoto K. and Tran M.Q. 2019 *Nucl. Fusion* **59** 073001
[16] Jelonnek J. *et al* 2017 *Fusion Eng. Des.* **123** 241–6
[17] Savoldi L., Avramidis K.A., Albajar F., Alberti S., Leggieri A. and Sanchez F. 2021 *Energies* **14** 8027
[18] Rzesnicki T., Piosczyk B., Kern S., Illy S., Jin J., Samartsev A., Schlaich A. and Thumm M. 2010 *IEEE Trans. Plasma Sci.* **38** 1141–9
[19] Ioannidis Z.C. *et al* 2020 *45th Int. Conf. on Infrared, Millimeter and Terahertz Waves (Irmmw-thz)* (*Buffalo, NY, USA*)
[20] Illy S. *et al 2023 30th IEEE Symp. on Fusion Engineering (SOFE 2023)*
[21] Ruess T., Gantenbein G., Ioannidis Z., Rzesnicki T., Wagner D., Thumm M. and Jelonnek J. 2022 *tm-Technisches Messen* **89** 85–96
[22] Kalaria P. *et al* 2016 *2016 German Microwave Conf. (Gemic)* (*Bochum, Germany*) pp 377–80
[23] Ruess T. *et al* 2020 *2020 45th Int. Conf. on Infrared, Millimeter, and Terahertz Waves (Irmmw-thz)* (*Buffalo, NY, USA*) pp 1–2
[24] Ruess T. *et al* 2019 *EPJ Web Conf.* **203** 04014
[25] Dumbrajs O., Idehara T., Iwata Y., Mitsudo S., Ogawa I. and Piosczyk B. 2003 *Phys. Plasmas* **10** 1183–6
[26] Ell B., Wu C., Gantenbein G., Illy S., Misko M.S., Pagonakis I.G., Weggen J., Thumm M. and Jelonnek J. 2023 *IEEE Trans. Electron Des.* **70** 1299–305
[27] Pagonakis I.G., Hogge J.-P., Alberti S., Avramides K.A. and Vomvoridis J.L. 2008 *IEEE Trans. Plasma Sci.* **36** 469–80
[28] Wu C., Pagonakis I.G., Avramidis K.A., Gantenbein G., Illy S., Thumm M. and Jelonnek J. 2018 *Phys. Plasmas* **25** 033108
[29] Wu C., Pagonakis I.G., Albert D., Avramidis K.A., Gantenbein G., Illy S., Thumm M. and Jelonnek J. 2019 *Phys. Plasmas* **26** 013108
[30] Avramidis K.A., Marek A., Chelis I., Ioannidis Z.C., Feuerstein L., Jelonnek J., Thumm M. and Tigelis I. 2023 *IEEE Trans. Electron Devices* **70** 1898–905
[31] Chelis I., Peponis D. and Zelkas A. 2022 *Phys. Plasmas* **29** 033103
[32] Ioannidis Z.C., Chelis I., Gantenbein G., Rzesnicki T. and Jelonnek J. 2020 *IEEE Trans. Electron Devices* **67** 5783–9
[33] Peponis D. *et al* 2024 EUROfusion Deliverable HCD-T.01.02-T007-D001, EUROfusion IDM, EFDA_D_2R64VK (available at: https://idm.euro-fusion.org/default.aspx?uid=2R64VK)
[34] Ioannidis Z.C. *et al* 2019 *Fusion Eng. Des.* **146** 349–52
[35] Erckmann V. *et al* 2007 *Fusion Sci. Technol.* **52** 291–312
[36] Bruschi A. *et al* 2023 *Fusion Eng. Des.* **194** 113727
[37] Garavaglia S. *et al* 2023 *J. Vac. Sci. Technol. B* **41** 044201
[38] Murphy J.A. 1987 *Int. J. Infrared Millim. Waves* **8** 1165–87
[39] Empacher L. and Kasparek W. 2001 *IEEE Trans. Antennas Propag.* **49** 483–93
[40] TICRA 2017 GRASP technical description (Knud Pontoppidan) (available at: www.ticra.com)
[41] Kasparek W., Fernandez A., Hollmann F. and Wacker R. 2001 *Int. J. Infrared Millim. Waves* **22** 1695–707
[42] Barabash V. ITER material proprieties handbook Pure_Cu_-_Electrical_Resistivity_24L79N_v1_1
[43] Wagner D., Leuterer F., Kasparek W. and Stober J. 2017 *J. Infrared Milli. Terahz Waves* **38** 191–205
[44] Spaeh P., Bruschi A., Fanale F., Franke T., Garavaglia S., Strauss D. and Tran M.-Q. 2022 *IEEE Trans. Plasma Sci.* **50** 4419–24
[45] Gantenbein G. *et al* 2014 *IEEE Trans. Electron Devices* **61** 1806–11
[46] Diamond Materials GmbH & Co (KG Freiburg) (available at: www.diamond-materials.com/en/)
[47] Aiello G. *et al* 2021 *IEEE Trans. Electron Devices* **68** 4669–74
[48] Heidinger R. *et al* 2007 *32nd Int. Conf. on Infrared, Millimeter and Terahertz Waves* (*Cardiff, UK*)
[49] Aiello G., Gantenbein G., Jelonnek J., Meier A., Scherer T., Schreck S., Strauss D. and Thumm M. 2022 *J. Nucl. Eng.* **3** 342–51
[50] Spaeh P. *et al* 2024 *IEEE Trans. Plasma Sci.* (https://doi.org/10.1109/TPS.2024.3353822)
[51] Marraco Borderas C., Xydou A., Birlan D., Chavan R., Clément A., Goodman T.P., Hogge J.-P., Mas Sánchez A., Noël M. and Torreblanca H. 2024 *Fusion Eng. Des.* **199** 114139